Electro-optics of graphene: Field-modulated reflection and birefringence

M. V. Strikha and F. T. Vasko*
Institute of Semiconductor Physics, NAS of Ukraine, Pr. Nauky 41, Kyiv 03028, Ukraine
(Received 4 December 2009; revised manuscript received 13 January 2010; published 9 March 2010)

The electro-optical response of graphene due to heating and drift of carriers is studied theoretically. Real and imaginary parts of the dynamic conductivity tensor are calculated for the case of effective momentum relaxation, when anisotropic contributions are small. We use the quasiequilibrium distribution of electrons and holes, characterized by the effective temperature of carriers and by concentrations, which are controlled by gate voltage and in-plane electric field. The geometry of normal propagation of probe radiation is considered; spectral and field dependences of the reflection coefficient and the relative absorption are analyzed. The ellipticity degree of the reflected and transmitted radiations due to small birefringence of a graphene sheet with current has also been determined.

DOI: 10.1103/PhysRevB.81.115413 PACS number(s): 78.67.Wj, 81.05.ue, 78.20.Jq

I. INTRODUCTION

The study of the electro-optical response both of bulk semiconductors and of heterostructures (see Refs. 1 and 2, respectively) is a convenient method to characterize these materials. Such a response is used to modulate both the intensity of radiation and its polarization. As it was demonstrated more than 30 years ago[3,4] (see also Sec. 17 in Ref. 5), the main contribution to the electro-optical response of narrow gap semiconductors is caused by the modulation of the interband transitions, both virtual and real ones, under heating and drift of nonequilibrium carriers. The electro-optical properties of two-dimensional carriers in heterostructures have also been studied.[6] Since graphene is a gapless semiconductor with linear energy spectrum,[7] the direct interband transitions in graphene are allowed with the characteristic interband velocity $v_W = 10^8$ cm/s, which corresponds the Weyl-Wallace model,[8] degenerated over spin and valleys. Therefore, optical properties of graphene should be modulated essentially by temperature and carriers' concentration,[9] and these dependences were studied recently.[10] The applied electric field changes not the carriers' temperature and concentration only, it also causes the anisotropy of distribution due to the carriers' drift.[11,12] Therefore, the birefringence effect can be essential for radiation propagating across a graphene sheet with current. To the best of our knowledge, no measurement of electro-optical response was performed until recently and a theoretical study of these phenomena is timely now.

The results obtained below are based on the tensor of dynamic conductivity determined by interband transitions of nonequilibrium carriers. This tensor is determined by the Kubo formula in collisionless approximation[4,5] with the use of weakly anisotropic distributions of electrons and holes calculated in Refs. 11 and 13. The case of normal propagation of the incident (in), reflected (r), and transmitted (t) waves of probe radiation (see Fig. 1; we consider the structure vacuum—graphene sheet—thick substrate with permittivity ϵ) is studied, and the reflection and transition coefficients, controlled by carriers' heating conditions, are obtained. It is demonstrated that the heating level dependence on applied field, temperature of phonons, and sheet charge, controlled by gate voltage V_g, can be verified from electro-optical measurements. Moreover, graphene is to be considered as a uniaxial plane due to carriers' drift and the elliptically polarized r and t waves appear under linear polarization of in-radiation, if $\theta \neq 0$ or $\pi/2$; see Fig. 1. The distribution anisotropy and the induced birefringence are small due to an effective relaxation of carriers' momenta, but a high sensitivity of polarization measurements enables one to determine drift characteristics of nonequilibrium carriers using a field-induced Kerr effect.

The consideration below is organized in the following way. In Sec. II we present both the basic equations for the complex tensor of dynamic conductivity and the electrodynamics equations for the uniaxial graphene sheet on a substrate. Numerical results, describing the electromodulation spectra and Kerr effect, are discussed in Sec. III. The concluding remarks and the list of assumptions are presented in the last section. In the Appendix, the dynamic conductivity of the undoped graphene is considered.

II. BASIC EQUATIONS

The description of graphene response on the probe in-plane electric field $\mathbf{E}_\omega \exp(-i\omega t)$ is based on the consideration of the high-frequency dynamic conductivity and on the examination of the electrodynamics problem for propagation of such a field through the graphene sheet. When performing

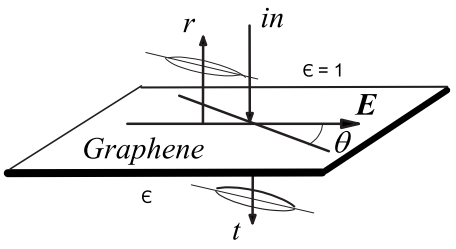

FIG. 1. Schematic view on incident (in), reflected (r), and transmitted (t) radiations for the case of normal propagation through the graphene sheet with applied electric field $\mathbf{E}$. Angle θ defines the polarization direction of in-wave while r and t contributions are elliptically polarized.

these calculations, we take into account a modification of interband transitions due to carriers' heating and an anisotropy of response due to carriers' drift.

A. Anisotropic dynamic conductivity

The contribution of the interband transitions of nonequilibrium carriers with the distribution function $f_{l\mathbf{p}}$ into the response at frequency ω is described by the dynamic conductivity tensor $\sigma_{\alpha\beta}(\omega)$ given by the Kubo formula:

$$\sigma_{\alpha\beta}(\omega) = i\frac{4(ev_W)^2}{\omega L^2}\sum_{ll'\mathbf{p}}(f_{l\mathbf{p}} - f_{l'\mathbf{p}})\frac{\langle l\mathbf{p}|\hat{\sigma}_\alpha|l'\mathbf{p}\rangle\langle l'\mathbf{p}|\hat{\sigma}_\beta|l\mathbf{p}\rangle}{\varepsilon_{lp} - \varepsilon_{l'p} + \hbar\omega + i\lambda}. \tag{1}$$

Here $|l\mathbf{p}\rangle$ and ε_{lp} are the state and energy of the lth band (c or v) with the 2D momentum $\mathbf{p}$, and $\lambda \to +0$. We also use the velocity operator $v_W\hat{\boldsymbol{\sigma}}$ and the normalizing area L^2. Expression (1) is written in a collisionless approximation $\omega\bar{\tau} \gg 1$ ($\bar{\tau}$ is the relaxation time), when intraband transitions are inefficient. In this case the density matrix, averaged over scattering, should be used in the Kubo formula and $\sigma_{\alpha\beta}(\omega)$ appears to be written through the stationary distribution function $f_{l\mathbf{p}}$.[5] Due to effective momentum relaxation the anisotropy of nonequilibrium electron and hole distributions is weak and the expansion

$$f_{l\mathbf{p}} = f_{lp} + \Delta f_{lp}^{(1)}\cos\varphi + \Delta f_{lp}^{(2)}\cos 2\varphi + \cdots \tag{2}$$

should be substituted into Eq. (1). Here the φ angle determines the orientation of $\mathbf{p}$, and $\Delta f_{lp}^{(r)} \propto E^r$, where $\mathbf{E} \| OX$ is a dc field applied. The linear in E contribution can be omitted from $\sigma_{\alpha\beta}(\omega)$ in the case, when the small spatial dispersion, responsible for the radiation drag by current (see Ref. 14), is neglected. Thus, with an accuracy of the contributions of $\propto E^2$ order, tensor (1) is determined by the transition matrix elements

$$\overline{|\langle 1\mathbf{p}|\hat{\sigma}_{x,y}|-1\mathbf{p}\rangle|^2} = 1/2,$$

$$\overline{\cos 2\varphi|\langle 1\mathbf{p}|\hat{\sigma}_x|-1\mathbf{p}\rangle|^2} = -1/4,$$

$$\overline{\cos 2\varphi|\langle 1\mathbf{p}|\hat{\sigma}_y|-1\mathbf{p}\rangle|^2} = 1/4, \tag{3}$$

where the overline means the averaging over angle.

Since the nondiagonal components of tensor (1) vanish, the XX and YY components of dynamic conductivity,

$$\sigma_{xx}(\omega) = \sigma_\omega - \frac{\Delta\sigma_\omega}{2}, \quad \sigma_{yy}(\omega) = \sigma_\omega + \frac{\Delta\sigma_\omega}{2}, \tag{4}$$

describe the response of the graphene sheet with the field-induced uniaxial anisotropy. Further, we substitute Eqs. (2) and (3) into Eq. (1) and we use the electron-hole representation, when $f_{c\mathbf{p}} \to f_{e\mathbf{p}}$, and $f_{v\mathbf{p}} \to 1 - f_{h,-\mathbf{p}}$; see Ref. 11. It is convenient to separate the contributions of the undoped graphene and of the free carriers (electrons and holes) into the isotropic part of conductivity, $\bar{\sigma}_\omega$ and $\sigma_\omega^{(c)}$, so that $\sigma_\omega = \bar{\sigma}_\omega + \sigma_\omega^{(c)}$. The first contribution is discussed in the Appendix. Separating the real and imaginary parts of $\bar{\sigma}_\omega$, and using the energy conservation law, one obtains the frequency-independent result $\mathrm{Re}\,\bar{\sigma} = e^2/4\hbar$. The imaginary contribution to $\bar{\sigma}_\omega$ is given by the phenomenological expression (A2), which is written through the fitting parameters, corresponding to the recent measurements.[15]

The electron-hole contributions to the isotropic part, $\sigma_\omega^{(c)}$, and the anisotropic addition, $\Delta\sigma_\omega$, are written as follows ($\mathcal{P}$ indicates the principal value of integrals):

$$\mathrm{Re}\begin{vmatrix}\sigma_\omega^{(c)}\\ \Delta\sigma_\omega\end{vmatrix} = -\frac{2\pi(ev_W)^2}{\omega L^2}\sum_{\mathbf{p}}\delta(\hbar\omega - 2v_W p)\begin{vmatrix} f_{ep} + f_{hp}\\ \Delta f_{ep}^{(2)} + \Delta f_{hp}^{(2)}\end{vmatrix}, \tag{5}$$

$$\mathrm{Im}\begin{vmatrix}\sigma_\omega^{(c)}\\ \Delta\sigma_\omega\end{vmatrix} = -\frac{2(ev_W)^2}{\omega L^2}\sum_{\mathbf{p}}\frac{\mathcal{P}}{\hbar\omega - 2v_W p}\frac{4v_W p}{\hbar\omega + 2v_W p}\begin{vmatrix} f_{ep} + f_{hp}\\ \Delta f_{ep}^{(2)} + \Delta f_{hp}^{(2)}\end{vmatrix}. \tag{6}$$

The real parts of the conductivity, given by Eq. (5), are expressed directly through isotropic distribution (2) at the characteristic momentum for interband transitions, $p_\omega \equiv \hbar\omega/2v_W$, according to

$$\mathrm{Re}\begin{vmatrix}\sigma_\omega^{(c)}\\ \Delta\sigma_\omega\end{vmatrix} = -\frac{e^2}{4\hbar}\begin{vmatrix} f_{ep_\omega} + f_{hp_\omega}\\ \Delta f_{ep_\omega}^{(2)} + \Delta f_{hp_\omega}^{(2)}\end{vmatrix}. \tag{7}$$

The imaginary parts of $\sigma_\omega^{(c)}$ and $\Delta\sigma_\omega$, given by Eq. (6), are transformed into

$$\mathrm{Im}\begin{vmatrix}\sigma_\omega^{(c)}\\ \Delta\sigma_\omega\end{vmatrix} = -\frac{e^2}{2\pi\hbar p_\omega}\int_0^\infty \frac{dpp^2}{p_\omega + p}\frac{\mathcal{P}}{p_\omega - p}\begin{vmatrix} f_{ep} + f_{hp}\\ \Delta f_{ep}^{(2)} + \Delta f_{hp}^{(2)}\end{vmatrix} \tag{8}$$

and the principal value integrals here should be calculated numerically.

Below, we restrict ourselves to the case of quasielastic distribution of nonequilibrium electrons and holes ($k = e, h$) with effective temperature T_c and chemical potential μ_k:

$$f_{kp} = \{\exp[(v_W p - \mu_k)/T_c] + 1\}^{-1}. \tag{9}$$

The dependences of distribution (9) on electric field E, temperature T, and gate voltage V_g are presented in Refs. 11 and 13. In the case of momentum relaxation through elastic scattering for the anisotropic addition $\Delta f_{k\mathbf{p}}^{(2)}$ we use

$$\Delta f_{kp}^{(2)} = -\frac{(eE)^2 p}{2\nu_p^{(2)}}\frac{d}{dp}\left[\frac{1}{p\nu_p^{(1)}}\left(-\frac{df_{kp}}{dp}\right)\right]. \tag{10}$$

For the case of short-range scattering on static defects the relaxation rates $\nu_p^{(1,2)}$ are proportional to the density of states, so that $\nu_p^{(1)} = v_d p/\hbar + \nu_0$ and $\nu_p^{(2)} = 2\nu_p^{(1)} + \nu_0$. Here v_d is a characteristic velocity, which determines an efficiency of momentum scattering,[16] and ν_0 is a residual rate, which describes the scattering process for low-energy carriers.

B. Electrodynamics

For normal propagation of probe radiation, the Fourier component of the field, $\mathbf{E}_{\omega z}$, is governed by the wave equation:

$$\frac{d^2\mathbf{E}_{\omega z}}{dz^2} + \epsilon_z\left(\frac{\omega}{c}\right)^2 \mathbf{E}_{\omega z} + i\frac{4\pi\omega}{c^2}\mathbf{j}_{\omega z} = 0, \tag{11}$$

where ϵ_z is the dielectric permittivity. In this paper we examine the case of graphene on the thick SiO_2 substrate, when $\epsilon_{z<0}=1$ and $\epsilon_{z>0}=\epsilon$. The induced current density in Eq. (11) is localized around $z=0$ plane, so that $\mathbf{j}_{\omega z} \approx \hat{\sigma}_{\omega z}\mathbf{E}_{\omega z=0}$, while $\int_{-0}^{+0} dz \hat{\sigma}_{\omega z} = \hat{\sigma}_\omega$ is determined through the dynamic conductivity tensor, being examined above. Outside the graphene sheet the solution of Eq. (11) can be written as

$$\mathbf{E}_{\omega z} = \begin{cases} \mathbf{E}^{(in)} e^{ik_\omega z} + \mathbf{E}^{(r)} e^{-ik_\omega z}, & z < 0 \\ \mathbf{E}^{(t)} e^{i\bar{k}_\omega z}, & z > 0. \end{cases} \tag{12}$$

Here the wave vectors $k_\omega = \omega/c$ and $\bar{k}_\omega = \sqrt{\epsilon}\omega/c$, and the amplitudes of incident, reflected, and transmitted waves ($\mathbf{E}^{(in)}$, $\mathbf{E}^{(r)}$, and $\mathbf{E}^{(t)}$, respectively) were introduced. These amplitudes are governed by the boundary condition

$$\frac{d\mathbf{E}_{\omega z}}{dz}\bigg|_{-0}^{+0} + ik_\omega \frac{4\pi}{c}\hat{\sigma}_\omega \mathbf{E}_{\omega z=0} = 0, \tag{13}$$

which is obtained after integration of Eq. (11) over z through the graphene layer ($-0 < z < +0$). The second boundary condition is the requirement of continuity: $\mathbf{E}_{\omega z=-0} = \mathbf{E}_{\omega z=+0}$.

Taking into account the diagonality of $\hat{\sigma}_\omega$ tensor, we get the solutions from the boundary conditions as follows:

$$E_\alpha^{(t)} = \frac{2}{1+A_\alpha(\omega)} E_\alpha^{(in)}, \quad E_\alpha^{(r)} = \frac{1-A_\alpha(\omega)}{1+A_\alpha(\omega)} E_\alpha^{(in)}, \tag{14}$$

where factor $A_\alpha(\omega) = \sqrt{\epsilon} + 4\pi\sigma_{\alpha\alpha}(\omega)/c$ was introduced. After substitution of Eqs. (12) and (14) into the general expression for Poynting vector $\mathbf{S} = c^2\,\mathrm{Re}[\mathbf{E}\times \mathrm{rot}\,\mathbf{E}^*]/8\pi$, we obtain the incident, reflected, and transmitted fluxes S_{in}, S_r, and S_t, respectively, which are parallel to OZ. After multiplication of Eq. (13) by $\mathbf{E}_t^*$, we get the relation between these fluxes as follows:

$$S_{in} = S_r + S_t + \frac{1}{2}\mathrm{Re}(\mathbf{E}_t^* \cdot \hat{\sigma}_\omega \cdot \mathbf{E}_t), \tag{15}$$

where the last term describes absorption.

The polarization characteristics of r and t waves are determined by solutions (14). It is convenient to present them in complex form $E_\alpha = \mathcal{E}_\alpha \exp(i\psi_\alpha)$, where $\mathcal{E}_\alpha$ and ψ_α give the amplitude and phase of the α component of the field, respectively. At $\theta=0$, or at $\theta=\pi/2$, when the response is described by σ_{xx}, or by σ_{yy}, the linearly modulated r and t waves occur. For other θ, the reflected and transmitted waves are elliptically polarized. The ellipticity degree $\varepsilon(\omega)$ is determined by the phase difference between X and Y components of the field, $\Delta\psi = \psi_x - \psi_y$; see the general expressions in Ref. 17. Under weak anisotropy, with the accuracy up to first order in $\Delta\sigma_\omega$, we get $\varepsilon(\omega) = \Delta\psi/2$.

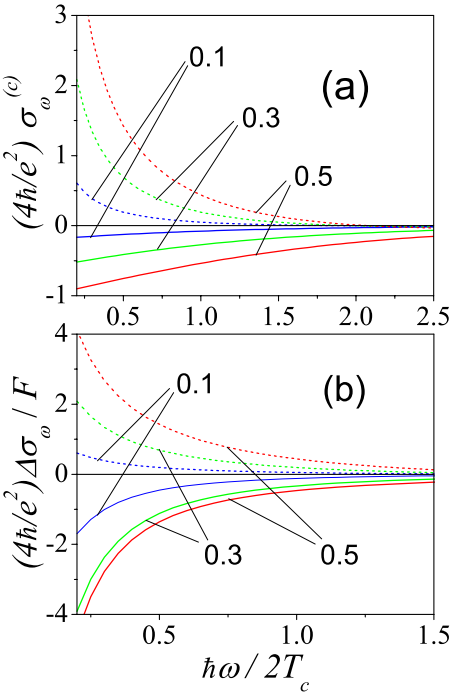

FIG. 2. (Color online) Spectral dependences of (a) $\sigma_\omega^{(c)}$ and (b) $\Delta\sigma_\omega$ for intrinsic graphene with $f_{p=0}=0.5$, 0.3, and 0.1. Solid and dashed curves correspond to real and imaginary parts of conductivity, respectively.

III. RESULTS

Now we examine the spectral and polarization characteristics of the electro-optical response. We study the reflection, transmission, and relative absorption coefficients determined as $R_{\omega\theta} = S_r/S_{in}$, $T_{\omega\theta} = S_t/S_{in}$, and $\xi_\omega = \mathrm{Re}(\mathbf{E}_t^* \cdot \hat{\sigma}_\omega \cdot \mathbf{E}_t)/2S_{in}$, respectively,[18] as well as the ellipticity degree, $\varepsilon(\omega)$, for the case of weak anisotropy. The final expressions for the coefficients under consideration are obtained with the use of complex conductivities $\sigma_\omega^{(c)}$ and $\Delta\sigma_\omega$ given by Eqs. (7) and (8), and they depend both on $\hbar\omega/T_c$ and on carriers' concentration. In Fig. 2 we plot these dependences, and one can see that the response modify essentially with temperature and concentration. The smallness of anisotropic additions is determined by dimensionless factor

$$F = \left(\frac{eE\hbar v_W^2}{2T_c^2 v_d}\right)^2, \tag{16}$$

which arises from $\propto E^2$ contribution to distribution function (10). Note also that Im $\Delta\sigma_\omega$ depends weakly on the cutting parameter $(\hbar\nu_0 v_W)/(T_c v_d)$ taken below as 0.1.

A. Reflection and absorption

For the examination of $R_{\omega\theta}$ and $\xi_{\omega\theta}$ it is convenient to separate the isotropic and θ-dependent contributions, so that

$$R_{\omega\theta} = R_\omega + \Delta R_\omega \cos 2\theta, \quad \xi_{\omega\theta} = \xi_\omega + \Delta\xi_\omega \cos 2\theta, \tag{17}$$

where the small (of the order of $\Delta\sigma_\omega/\sigma_\omega$) anisotropic additions, proportional to $\cos 2\theta$, have been separated, see Fig. 1, where θ is introduced as an angle between the polarization

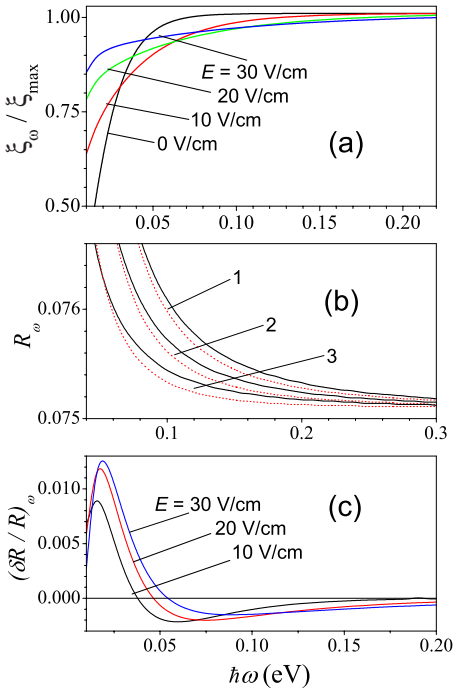

FIG. 3. (Color online) Spectral dependencies of (a) relative absorption, (b) reflection, and (c) differential reflectivity for intrinsic graphene at 77 K and at different electric fields, E (marked). Solid and dashed curves in (b) are plotted at $E=0$ and 30 V/cm, respectively, for $\varepsilon_m=60$ meV (1), 80 meV (2), and 100 meV (3).

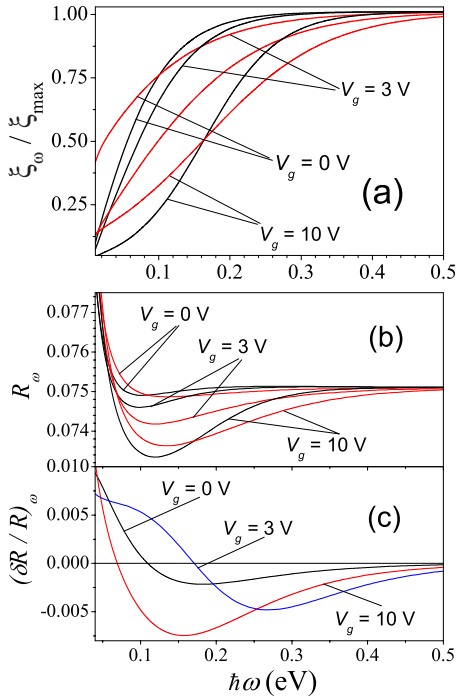

FIG. 4. (Color online) The same as in Fig. 3 for doped graphene at room temperature and different V_g (marked). Solid and dashed curves correspond to $E=0$ and 30 V/cm, respectively.

and field directions. The coefficients in Eq. (17) are written below through σ_ω, $\Delta\sigma_\omega$, and the factor $A_\omega=\sqrt{\epsilon}+4\pi\sigma_\omega/c$. For the isotropic parts of reflection and relative absorption coefficients we get[9]

$$R_\omega \simeq \left|\frac{1-A_\omega}{1+A_\omega}\right|^2, \quad \xi_\omega \simeq \frac{16\pi}{\sqrt{\epsilon}c}\frac{\mathrm{Re}\,\sigma_\omega}{|1+A_\omega|^2}, \tag{18}$$

so that these characteristics depend on T, E, and V_g.

The spectral dependences of the relative absorption, $\xi_\omega/\xi_{\max}$, the reflection, R_ω, and the differential reflectivity $(\delta R/R)_\omega \equiv (R_\omega - R_\omega^{(eq)})/R_\omega^{(eq)}$, are plotted in Fig. 3 for intrinsic graphene at $T=77$ K and at different electric fields (the data for T_c and carriers' concentration were used from Ref. 11). Here $\xi_{\max}$ is the maximum value of relative absorption for high frequencies, when the free carriers' contribution is unessential. One can see that due to the increase in average energy of carriers with the increase in E the absorption increases at high frequencies and decreases for the low ones. The relative change in ξ_ω is reasonably large and for $\hbar\omega \sim T_c$ it can be measured directly. At the same time, the reflection coefficient depends on the field in more weak ways, see Figs. 3(b) and 3(c), and $(\delta R/R)_\omega$ can be 10^{-2} in the terahertz spectral region; in the near-IR spectral region it decreases down to value $\leq 10^{-3}$. Note that for $\hbar\omega \leq 0.1$ eV R_ω increases essentially (at high frequencies $R_\omega \sim 0.075$) due to the contribution of the first summand of Eq. (A2). Figure 3(b) presents the dependence of R_ω on phenomenological parameter ε_m; ξ_ω depends weakly on this parameter.

The dependences of ξ_ω, R_ω, and $(\delta R/R)_\omega$ on the doping level are presented in Fig. 4. The data for the room temperature are presented for $V_g=3$ V and 10 V, which correspond to the difference between electron and hole concentrations 1.65×10^{11} cm^{-2} and 5.5×10^{11} cm^{-2}, respectively. Similarly to field dependences at $T=77$ K (see Fig. 3), the response moves toward the high-energy region with the increase in V_g (the doping level $\propto V_g$). The dependences on the level of heating (the applied field E) and on carriers' concentration (the gate voltage V_g) correspond to the measurements of spectra for different temperatures and V_g; see Ref. 10. For the range of parameters under examination, the field modulation of ξ_ω is of 20%–50% order up to the mid-IR spectral region. These modifications should be observed rather easily. The carriers' contribution to reflection increases as well: at $\hbar\omega > 0.1$ eV the decrease in R_ω occurs and R_ω almost does not depend on ε_m; in this case the shape of the differential reflectivity is similar to the low-temperature case, with the shift into the high-energy region.

Later we shall examine the anisotropic contributions in Eq. (17), which are proportional to $\Delta\sigma_\omega$. Such a contribution to reflection coefficient is given by

$$\Delta R_\omega = \frac{R_\omega}{c}\left(\frac{4\pi\Delta\sigma_\omega}{1-A_\omega^2}+\mathrm{c.c.}\right) \tag{19}$$

and the addition to relative absorption takes the form

$$\Delta\xi_\omega = \frac{16\pi}{\sqrt{\epsilon}c}\frac{\mathrm{Re}\,\sigma_\omega}{|1+A_\omega|^2}\left(\frac{2\pi\Delta\sigma_\omega/c}{1+A_\omega}+\mathrm{c.c.}\right) - \frac{16\pi}{\sqrt{\epsilon}c}\frac{\mathrm{Re}\,\Delta\sigma_\omega}{|1+A_\omega|^2}. \tag{20}$$

The spectral dependences for anisotropic contributions to the relative absorption and reflectivity, $\Delta\xi_\omega/F$ and $\Delta R_\omega/(R_\omega F)$,

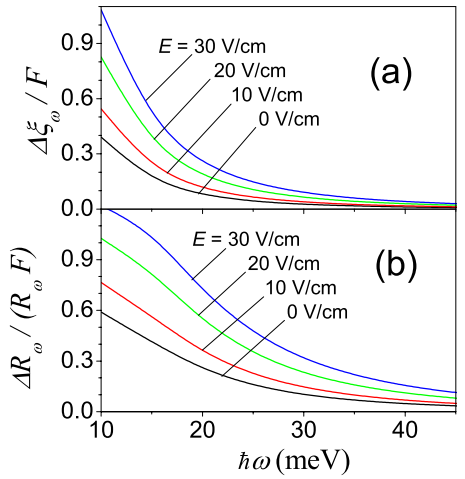

FIG. 5. (Color online) Spectral dependences of anisotropic contributions to relative absorption, (a) $\Delta\xi_\omega/F$, and to reflectivity, (b) $\Delta R_\omega/(R_\omega F)$, for intrinsic graphene at $T=300$ K and at different electric fields, E.

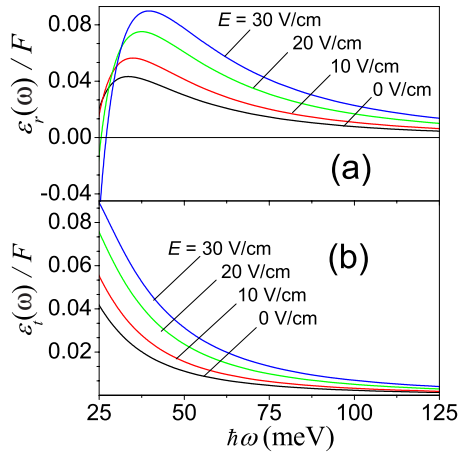

FIG. 6. (Color online) Spectral dependences of ellipticity degrees of r and t waves [panels (a) and (b), respectively] for intrinsic graphene at $T=300$ K and at different electric fields, E.

are shown in Figs. 5(a) and 5(b). One can see that in the range of fields under examination the parameter F given by Eq. (16) does not exceed 0.05, so that $\Delta\xi_\omega$ and $\Delta R_\omega/R_\omega$ are of 10^{-4} order for the mid-IR spectral region ($\sim 0.1-0.2$ eV) and the response increases up to $\sim 10^{-2}$ in the terahertz spectral region. The anisotropy of such order of value can be analyzed with the use of modulation methods.

B. Kerr effect

Besides the cases of parallel or transverse orientation of the probe radiation polarization with respect to the drift direction (i.e., at $\theta \neq 0,\ \pi/2$), the reflected and transmitted fields are polarized elliptically. The maximal Kerr effect occurs if the i wave is polarized along $\theta=\pi/4$ and below we consider this case only. In the approximation of the weakly anisotropic distribution (2) the ellipse orientation does not differ essentially from $\theta \simeq \pi/4$ and the ellipticity degree can be written as[17]

$$\varepsilon(\omega) = \sin\beta\ \mathrm{Re}\ \Phi(\omega) - \cos\beta\ \mathrm{Im}\ \Phi(\omega). \tag{21}$$

Here the β angle and the complex function $\Phi(\omega)$ can be expressed through the difference of the phases of r and t waves (see the end of Sec. II). The smallness of the ellipticity is determined by the relation $\Phi(\omega) \propto F$, while the β angle is not small.

For the reflected wave the $\Phi(\omega)$ function is given by the expression

$$\Phi_r(\omega) = \frac{4\pi\Delta\sigma_\omega}{c(1+A_\omega)^2}\left|\frac{1+A_\omega}{1-A_\omega}\right|, \tag{22}$$

while the β angle is introduced through the relation

$$\tan\beta_r = -\frac{2\ \mathrm{Im}\ A_\omega}{1-|A_\omega|^2}. \tag{23}$$

Similarly, for the transmitted wave, Eq. (20) is expressed through the function

$$\Phi_t(\omega) = \frac{2\pi\Delta\sigma_\omega}{c(1+A_\omega)^2}|1+A_\omega| \tag{24}$$

and the β angle is given by the expression

$$\tan\beta_t = -\frac{\mathrm{Im}\ A_\omega}{1+\mathrm{Re}\ A_\omega}. \tag{25}$$

Substitution of these expressions into Eq. (21) gives the ellipticity degrees for r and t waves, $\varepsilon_r(\omega)$ and $\varepsilon_t(\omega)$.

The spectral and field dependences of $\varepsilon_r(\omega)$ and $\varepsilon_t(\omega)$ are shown in Figs. 6(a) and 6(b) for intrinsic graphene at $T=300$ K. In the mid-IR spectral region $\varepsilon_{r,t}(\omega)$ decreases with ω, so that for $\hbar\omega \sim 0.1-0.2$ eV the value of ellipticity degree does not exceed $\sim 10^{-4}$ at $F \sim 0.05$. In the terahertz spectral region $\varepsilon_{r,t}(\omega)$ increases up to $\sim 5\times 10^{-3}$, wherein the direction of rotation for the reflected wave changes at $\hbar\omega \sim 25$ meV. Such a value of ellipticity degree can be detected by modulation methods only. However, in stronger fields, when the distribution function is strongly anisotropic,[12] the ellipticity degree can increase essentially.

IV. CONCLUSIONS

Summarizing the consideration presented, the examination of the graphene electro-optical response due to the interband electron transitions under the carriers' heating and drift is performed and a measurable size of these effects is demonstrated. It was found that an essential modulation of the reflection and the relative absorption take place starting from the field strength ~ 30 V/cm at liquid nitrogen and room temperatures (with the increase in field, the modulation should increase essentially). The weak ellipticity of the reflected and transmitted radiations arises due to current-induced birefringence of the graphene sheet.

Next, we list and discuss the assumptions used in our calculations. First, the dynamic conductivity tensor (1) is written in collisionless approximation. For the case of short-range scattering, when $\omega \gg v_d p_\omega/\hbar$, one arrives to the condition $v_d/2v_W \ll 1$, and the collisionless approximation is not

valid for a strongly disordered material. Also, the interband response of a pure graphene is described with the use of the phenomenological expression (A2) and a low-frequency restriction for this approximation is not clear.

Second, the quasiequilibrium distribution of carriers (9) was used for the numerical estimation of electro-optical response. This means the assumption of an effective intercarrier scattering. The complete description of the carriers' heating under such conditions had not been performed yet.[11,19] However, approximation (9) gives a good estimation for the response magnitude and the peculiarities of spectral dependences enable us to determine the contributions of the different relaxation mechanisms. Similarly, the use of the short-range scattering model in the drift-induced contribution (10) gives the estimation for optical anisotropy magnitude, and the spectral dependences' peculiarities contain information about the momentum relaxation mechanism (despite the short-range scattering that can be treated as a dominant one within the phenomenological description of momentum relaxation,[16] the microscopic mechanism has not been verified until now[20]).

Third, we have examined the heating of carriers with low energies only (the results for $E \leq 30$ V/cm have been presented), while the essential electro-optical response occurs in the terahertz spectral region only. With the increase in field (up to tens of kilovolts per centimeter; see Ref. 12) the electro-optic effect increases and shifts into the near-IR spectral region. The theoretical approach developed here can be applied for this region as well; however, the calculation of the distribution of hot carriers for this case has not been performed yet.

Fourth, the case of graphene on a thick substrate has been examined. The consideration of the interference effects for graphene, placed on a substrate of limited thickness, needs more complicated calculations and is beyond the frame of this paper. It is because the wavelength exceeds a typical layer thickness and the interference is negligible at $\hbar\omega \leq 0.1$ eV. However, an accuracy of measurements increases for the mid-IR (starting $\hbar\omega \sim 0.4$ eV) and optical spectral regions,[21] and the electro-optical effect under these conditions will be considered elsewhere. And the last, we have limited ourselves to the examination of the geometry of normal propagation of radiation only. The study of the response dependence on the angle of radiation falling gives additional experimental data; however, it is more complicated and needs special treatment.

Finally, the results obtained demonstrate that the electro-optical response due to heating and drift of carriers is large enough and it can be measured (similar measurements are possible for multilayer graphene structures). Because of strong dependence of the response on the applied field, temperature, and gate voltage, these measurements can give information on relaxation and recombination mechanisms. In addition, the electro-optical response of graphene can be applied for modulation of intensity and polarization of radiation in the terahertz and mid-IR spectral regions.

APPENDIX: RESPONSE OF UNDOPED GRAPHENE

The dynamic conductivity for the case of undoped graphene is described by Eqs. (1) and (3) after replacement of $f_{v\mathbf{p}}$ by 1 and of $f_{c\mathbf{p}}$ by 0. As a result we get the expression

$$\bar{\sigma}_\omega = \frac{2(ev_W)^2}{\omega L^2}\sum_{\mathbf{p}}\left[\pi\delta(\hbar\omega - 2v_W p) + i\mathcal{P}\frac{4v_W p}{(\hbar\omega)^2 - (2v_W p)^2}\right], \tag{A1}$$

where the real and imaginary parts of conductivity have been separated. The direct integration with the use of the energy conservation law gives the frequency-independent real part of Eq. (A1): $\mathrm{Re}\,\bar{\sigma} = e^2/4\hbar$. The imaginary contribution to $\bar{\sigma}_\omega$ appears to be divergent at $p \to \infty$; moreover, $\mathrm{Im}\,\bar{\sigma}_\omega \propto v_W p_m/\hbar\omega$, where p_m is a cutoff momentum.[22] Contrary to the case of bulk material,[9] this cutoff appears to be too rough for the description of the response in graphene. It is convenient to approximate $\mathrm{Im}\,\bar{\sigma}_\omega$ by separating the terms $\propto\omega^{-1}$ and $\propto\omega$, which correspond to the contributions of the virtual interband transitions and of ions correspondingly. As a result, we get

$$\mathrm{Im}\,\bar{\sigma}_\omega \approx \frac{e^2}{\hbar}\left(\frac{\varepsilon_m}{\hbar\omega} - \frac{\hbar\omega}{\varepsilon_i}\right), \tag{A2}$$

where the characteristic energies ε_m and ε_i have been introduced. The comparison of the response, described by $\bar{\sigma}_\omega$, with the recent measurements of the graphene optical spectra, yields $\varepsilon_m \sim 0.08$ eV and $\varepsilon_i \sim 6.75$ eV.[15]

*ftvasko@yahoo.com

[1] M. Cardona, *Modulation Spectroscopy* (Academic Press, New York, 1969).

[2] F. T. Vasko and A. V. Kuznetsov, *Electron States and Optical Transitions in Semiconductor Heterostructures* (Springer, New York, 1998).

[3] L. E. Vorobev, V. G. Komissarov, V. I. Stafeev, and A. Yu. Ushakov, JETP Lett. **13**, 98 (1971); L. E. Vorobjev, D. V. Donetski, and D. A. Firsov, *ibid.* **59**, 869 (1994).

[4] F. T. Vasko, Fiz. Tverd. Tela (Leningrad) **15**, 1693 (1973) [Sov. Phys. Solid State **15**, 1136 (1973)]; L. A. Almazov and I. M. Dykman, Phys. Status Solidi B **48**, 503 (1971).

[5] F. T. Vasko and O. E. Raichev, *Quantum Kinetic Theory and Applications* (Springer, New York, 2005).

[6] D. A. B. Miller, D. S. Chemla, T. C. Damen, A. C. Gossard, W. Wiegmann, T. H. Wood, and C. A. Burrus, Phys. Rev. B **32**, 1043 (1985); A. Fainstein, P. Etchegoin, P. V. Santos, M. Cardona, K. Totemeyer, and K. Eberl, *ibid.* **50**, 11850 (1994); L. E. Vorob'ev, D. A. Firsov, V. A. Shalygin, and I. I. Saidashev, JETP Lett. **65**, 549 (1997).

[7] A. H. Castro Neto, F. Guinea, N. M. R. Peres, K. S. Novoselov, and A. K. Geim, Rev. Mod. Phys. **81**, 109 (2009).

[8] P. R. Wallace, Phys. Rev. **71**, 622 (1947); E. M. Lifshitz, L. P. Pitaevskii, and V. B. Berestetskii, *Quantum Electrodynamics*

(Butterworth-Heinemann, London, 1982).
[9] L. A. Falkovsky, Phys. Usp. **51**, 887 (2008); T. Stauber, N. M. R. Peres, and A. K. Geim, Phys. Rev. B **78**, 085432 (2008).
[10] F. Wang, Y. Zhang, C. Tian, C. Girit, A. Zettl, M. Crommie, and Y. R. Shen, Science **320**, 206 (2008); R. R. Nair, P. Blake, A. N. Grigorenko, K. S. Novoselov, T. J. Booth, T. Stauber, N. M. R. Peres, and A. K. Geim, *ibid.* **320**, 1308 (2008); K. F. Mak, M. Y. Sfeir, Y. Wu, C. H. Lui, J. A. Misewich, and T. F. Heinz, Phys. Rev. Lett. **101**, 196405 (2008).
[11] O. G. Balev, F. T. Vasko, and V. Ryzhii, Phys. Rev. B **79**, 165432 (2009).
[12] J. Moser, A. Barreiro, and A. Bachtold, Appl. Phys. Lett. **91**, 163513 (2007); I. Meric, M. Y. Han, A. F. Yang, B. Ozyilmaz, P. Kim, and K. L. Shepard, Nat. Nanotechnol. **3**, 654 (2008); A. Barreiro, M. Lazzeri, J. Moser, F. Mauri, and A. Bachtold, Phys. Rev. Lett. **103**, 076601 (2009).
[13] O. G. Balev and F. T. Vasko (unpublished).
[14] T. S. Moss, G. J. Burrel, and A. Hetherington, Proc. R. Soc. London, Ser. A **308**, 125 (1968); L. A. Almazov, F. T. Vasko, and I. M. Dykman, JETP Lett. **16**, 214 (1972); L. E. Vorob'ev, D. V. Donetskii, and D. A. Firsov, *ibid.* **71**, 331 (2000).
[15] M. Bruna and S. Borini, Appl. Phys. Lett. **94**, 031901 (2009).
[16] F. T. Vasko and V. Ryzhii, Phys. Rev. B **76**, 233404 (2007).
[17] M. Born and E. Wolf, *Principles of Optics* (Pergamon Press, London, 1980).
[18] According to Eq. (15), the reflection, transmission, and relative absorption coefficients are connected by the relation $1=R_{\omega\theta}+T_{\omega\theta}+\xi_{\omega\theta}$.
[19] A. Akturk and N. Goldsman, J. Appl. Phys. **103**, 053702 (2008); R. S. Shishir and D. K. Ferry, J. Phys.: Condens. Matter **21**, 344201 (2009).
[20] L. A. Ponomarenko, R. Yang, T. M. Mohiuddin, M. I. Katsnelson, K. S. Novoselov, S. V. Morozov, A. A. Zhukov, F. Schedin, E. W. Hill, and A. K. Geim, Phys. Rev. Lett. **102**, 206603 (2009); S. Adam, P. W. Brouwer, and S. Das Sarma, Phys. Rev. B **79**, 201404(R) (2009).
[21] P. Blake, K. S. Novoselov, A. H. Castro Neto, D. Jiang, R. Yang, T. J. Booth, A. K. Geim, and E. W. Hill, Appl. Phys. Lett. **91**, 063124 (2007); D. S. L. Abergel, A. Russell, and V. I. Fal'ko, *ibid.* **91**, 063125 (2007); V. Yu and M. Hilke, *ibid.* **95**, 151904 (2009).
[22] A. Principi, M. Polini, and G. Vignale, Phys. Rev. B **80**, 075418 (2009); M. Polini, A. H. MacDonald, and G. Vignale, arXiv:0901.4528 (unpublished).